Higgs-mode signature in ultrafast electron dynamics in superconducting graphene

S. Pashalou,[1] H. Goudarzi [●],[1] M. Khezerlou,[2] and S. A. Jafari[3]

[1]*Department of Physics, Faculty of Science, Urmia University, P.O. Box 165, Urmia 5756151818, Iran*
[2]*Engineering Faculty of Khoy, Urmia University of Technology, Urmia 57166-17165, Iran*
[3]*Department of Physics, Sharif University of Technology, Tehran 11155-9161, Iran*

We theoretically investigate the effect of superconductivity on the ultrafast electron dynamics in graphene interacting with an ultrashort linearly polarized optical pulse. The optical pulse, with frequency greater than 1 THz, quadratically couples to the Higgs (amplitude) mode and therefore can excite the Higgs-mode oscillations in superconductors, leading to quenching superconducting excitation energy, even in *s*-wave pairing symmetry. Since the duration of the used pulse is less than the electron scattering time in graphene (10–100 fs), the electron dynamics driven by the electric field of pulse remains coherent and is described within the tight-binding model of graphene. We show that the electron-electron and hole-hole transitions from valence to conduction bands are substantially irreversible, with a large residual population of the conduction band, which implies quantum electron dynamics being highly nonadiabatic. Such a feature of the system allows us to clearly project the effect of Higgs oscillations on the electric dipole moment created by the electric field of the pulse between the conduction and valence bands. In particular, we study the impact of the superconducting pair potential on the conduction band population, where the strong pulse causes electronlike and holelike quasiparticles transitions between the conduction and valence bands. The conduction band electron redistribution in honeycomb Dirac points results in almost asymmetric hot spots in two different K and K' valleys after the pulse ends, which may be interpreted as the valley polarization effect due to the presence of superconductivity. The redistribution of hot spots around Dirac points is in good agreement with the Higgs-mode oscillations (corresponding to the electric dipole moment pattern), and the number of spots weakly depends on the superconducting gap, whereas it has a strong dependence on the ultrashort-pulse intensity.

I. INTRODUCTION

Despite the very long history of Higgs (amplitude) modes in superconductors, the scalar (and hence chargeless) nature of these modes prevents their linear coupling via minimal substitution to the external electromagnetic fields, and therefore, the experimental detection of the dynamics of the Higgs mode remained elusive and had to await technological developments of nonlinear and ultrafast laser technology [1]. Recent developments in ultrafast laser technology have created unique platforms to explore the coherent control of electron dynamics in solids at ultrafast timescales with high temporal resolution [1–10]. The electric field of such optical pulses is strong ($\approx$1 V/Å) and comparable to the internal fields in solids [11–13]. Such strong electric field can lead to emerging specific dynamical behaviors in materials and can be used in optical probing of electron dynamics in solids at femtosecond timescales [2,13,14]. In particular, among solids, two-dimensional (2D) crystalline materials, such as graphene [15,16], represent unique and peculiar physical properties due to the restriction of electron dynamics to a plane, actually leading to linear energy dispersion in the first Brillouin zone [17]. Specifically, the Dirac-like behavior of electrons in the honeycomb lattice of graphene causes the appearance of irreversible electron dynamics through interaction with a strong ultrafast optical pulse. In the last few years, several experimental and theoretical investigations have been carried out to study ultrafast nonlinear electron dynamics in 2D materials under ultrashort pulse irradiation [18–32]. The presence of two nondegenerate Dirac points, K and K', at the corners of the Brillouin zone potentially makes graphene a suitable platform to investigate novel (valley-dependent) ultrafast dynamics of zero effective mass electrons interacting with a ultrashort pulse [17,33]. In graphene, linearly polarized pulse induction causes the manifestation of interference fringes in the reciprocal space owing to band electron transitions around the Dirac points.

On the other hand, over the last few years, electronlike and holelike quasiparticle excitations in 2D materials in the presence of a proximity-induced superconducting order have been the subject of extensive theoretical and experimental research related to the spin-valley coupling resolved transport of charge carriers [34–37]. It was experimentally shown that the superconductivity may be induced by means of the proximity effect by placing a superconducting electrode near a graphene layer [38–42]. Therefore, here, significant attention is being devoted to ultrafast electron dynamics in an electron-hole pair (as well as the formation of the superconducting gap in the Fermi surface) caused by the electric field of a femtosecond optical pulse. However, it has been noticed that the superconducting

gap magnitude is very small compared to the ultrashort pulse. But importantly, the ultrashort pulse may really result in the appearance of an impulsive excitation of Higgs oscillations via a nonlinear process by quenching the electron-hole energy excitations in superconductors [43–46]. Higgs oscillations can be understood as massive (gapped) excitations along the radial direction around the Fermi point in the superconducting state. Such a quantum quench was first demonstrated in the *s*-wave symmetry superconducting order [43–46], despite the lack of dependence of the superconducting gap on the pair momentum. Also, recently, Higgs oscillations were characterized in unconventional superconductors with explicit dependency of the superconducting gap on the pair momentum [47]. Therefore, this effect can straightforwardly affect the ultrafast electron dynamics in the quantum transition between the valence and conduction bands in materials with a superconducting proximity effect under irradiation of an ultrashort laser pulse.

However, recently, valuable studies have begun in this field (see Refs. [47,48]). The authors of [48] reported universal control of the order parameter and handedness of chiral superconductors by optical pumping. The important properties of their predictions are that the mechanism extends to ultrafast timescales and the ensuing engineered state persists after the pump is switched off. They predicted that these phenomena can appear in graphene [49–51]. Moreover, they showed that the chiral superconductor can be achieved in time-resolved pump-probe measurements. Accordingly, we proceed in this paper to study the electron dynamics in the presence of the superconducting gap in graphene under irradiation of an ultrashort laser pulse. The superconducting gap is assumed to be a proximity-induced *s*-wave symmetry, which has no dependence on the pair momentum. We show that in the presence of the superconductivity effect, the quantum electron dynamics in graphene is still highly nonadiabatic and effectively irreversible. Moreover, the resulting irreversible electron dynamics leads to considerable electron transition from the valence band (VB) to the conduction band (CB), which results in a high electron population in the conduction band. The unique properties of ultrafast electron dynamics in graphene are given by specific features of the electric dipole moment, which lead to the associated singularities at the Dirac nodes in the Brillouin zone. Such singularities arise from the band touching, which result in the formation of highly localized hot spots for electron redistribution in the reciprocal honeycomb space, which actually is weakly dependent on the magnitude of the superconducting gap. Remarkably, the superconducting order parameter, which occupies off-diagonal elements of the Dirac–Bogoliubov–de Gennes (DBdG) graphene Hamiltonian for two different valleys, gives rise to a significant change in the resulting time-dependent conduction band population (CBP) owing to the formation of the Higgs mode.

However, the recent advances in ultrafast laser pulses and nonlinear techniques provide tools to access the real-time dynamics of low-energy excitations in superconductors. For example, time-resolved terahertz (THz) spectroscopy and time- and angular-resolved photoemission spectroscopy (tr-ARPES) have enabled us to detect the real-time dynamics of the superconducting gap amplitude. Here, photoexcitation with light whose frequency is larger than $2\Delta_s$ (Δ_s is the

superconducting gap energy) breaks a small portion of the Cooper pairs and gives rise to excess quasiparticle density. The relaxation proceeds via quasiparticle recombination, in which quasiparticle pairs recombine to form Cooper pairs by the emission of phonons with energy $\hbar\omega > 2\Delta_s$. Below the critical temperature of the superconductor, ultrafast excitations can trigger a synchronous decrease in the electron self-energy and superconducting gap. In our work, this scenario will be important when the superconducting order is taken to have *p*- or *d*-wave symmetry, for which the time dependence of the pair momentum (originating from the coupling with the electric field of the pulse) will play a crucial role in the CB transition rate. Note that as far as the response of the Dirac part of the spectrum of graphene is concerned, the Dirac theory is scale invariant. Specifically, for a realistic graphene material, scaling the energy from approximately eV down to approximately meV and below corresponds to dealing with momentum scales closer and closer to the Dirac node (and hence larger lattice sizes). This scale invariance means that moderate lattice sizes in the numerical solution of the coupled differential equations giving the dynamics of the electron-hole will be able to clearly capture the Higgs excitations. The outline of the present paper is as follows: Sec. II is devoted to the analytical solution of the DBdG equation with the *s*-wave order parameter to obtain the exact expressions for the energy dispersion and corresponding wave functions. Then, we introduce the related formalism to obtain the form of the dipole matrix elements and the exact relation of the time-dependent CBP that takes into account the Gaussian femtosecond optical pulse contribution to the momentum of electron. The results and discussion of the total transition rate for Dirac points in reciprocal space and the effect of superconductivity on CBP are presented in Sec. III. Finally, a brief conclusion is given.

II. THEORETICAL FORMALISM

A. Superconducting graphene lattice

Monolayer graphene has a hexagonal crystal structure made of two sublattices, A sites and B sites, which is shown in Fig. 1(a) [15,16]. These lattices are determined by two lattice vectors, $\mathbf{a}_1 \equiv a/2(3, \sqrt{3})$ and $\mathbf{a}_2 \equiv a/2(3, -\sqrt{3})$, where $a = 1.42$ Å is the lattice constant. The first Brillouin zone of the reciprocal lattice of graphene is shown in Fig. 1(b). The electron band structure in graphene's reciprocal space is determined by its spatial and time-reversal symmetries. The points $K \equiv (2\pi\sqrt{3}a/3)(\sqrt{3}, 1)$ and $K' \equiv (2\pi\sqrt{3}a/3)(\sqrt{3}, -1)$, which are the corners of graphene's first Brillouin zone, are the Dirac points. We consider a linearly polarized irradiated femtosecond pulse to the plane of monolayer graphene with a superconductor electrode on top of it, as shown in Fig. 2. The pulse is polarized along the *x* axis and has the following Gaussian wave shape:

$$F(t) = F_0(1 - 2u^2)e^{-u^2}. \tag{1}$$

Here, F_0 is the amplitude of the pulse oscillation, and $u = t/\tau$, where τ is the pulse's duration, which we set as $\tau = 1$ fs in calculations. The experimentally realized wave form of the ultrafast pulse can be found in Ref. [13]. For the shape of the pulse given by Eq. (1), which is shown in Fig. 3, the area
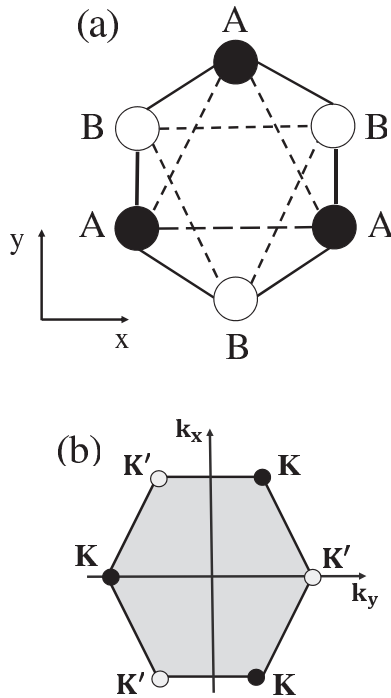
FIG. 1. (a) The honeycomb lattice of graphene is made of two triangular sublattices, A (black circles) and B (white circles). (b) The first Brillouin zone of the reciprocal lattice of graphene has two valleys, K and K', located at its boundaries.

under the pulse is always zero, $\int_{-\infty}^{+\infty} F(t)dt = 0$. It should be mentioned that the y axis is the axis of symmetry of graphene.

The time-dependent Hamiltonian of an electron subjected to a pulse electric field while taking into account the super-
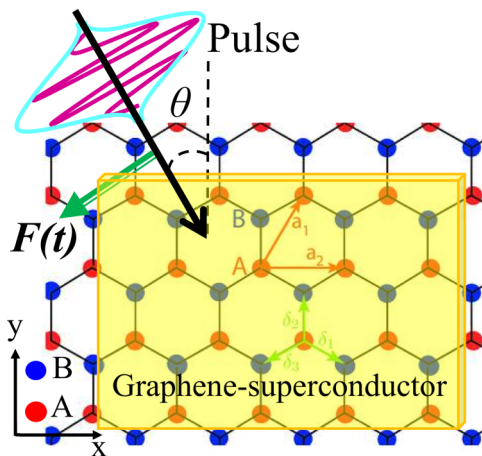

FIG. 2. Hexagonal lattice structure of monolayer graphene, which is illuminated by an ultrafast optical pulse associated with a strong electric field making an angle θ with the normal direction on the graphene plane. The graphene lattice consists of two inequivalent sublattices, labeled A (red circles) and B (blue circles). The vectors $\mathbf{a}_1 \equiv a/2(3, \sqrt{3})$ and $\mathbf{a}_2 \equiv a/2(3, -\sqrt{3})$ are the direct lattice vectors of graphene. The vectors δ_i ($i = 1, 2, 3$) are the lattice band parameters of graphene. The graphene superconductor is provided by a proximity effect of a superconductor electrode on top of the graphene.
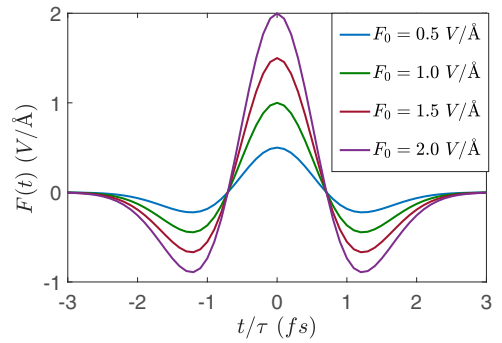

FIG. 3. Plot of different Gaussian wave forms of the electric field of the zero-area optical pulse as a function of time for various amplitude of F_0. Note that the pulse always has zero area, which satisfies the requirement of the pulse to propagate in the far-field zone.

conductivity effect has the form

$$\mathcal{H}(t) = \mathcal{H}_0^{\mathrm{DBdG}} + e\mathbf{F}(t) \cdot \mathbf{r}, \tag{2}$$

where $\mathcal{H}_0^{\mathrm{DBdG}}$ is the DBdG Hamiltonian for superconducting graphene, which determines the electron dynamics in the periodic lattice potential of graphene. $\mathbf{r} \equiv (x, y)$ is a 2D vector in the plane of graphene, e is the electron charge, and $\mathbf{F}(t) \equiv F(t)(\cos\theta, \sin\theta)$ is the external electric field of the pulse. We assume that the pulse is polarized along the x axis; that is, we consider the case of $\theta = 0$. Clearly, the presence of an electric field along the x axis breaks the $x \to -x$ mirror symmetry of the Dirac equation. Such symmetry breaking will be important beyond the linear response which is the case in our problem, as highly nonlinear excitations become possible. We will see that this feature will be directly observed in the response of different valleys.

Now, we proceed to consider the tight-binding Hamiltonian for graphene in the presence of a superconducting order. The full Hamiltonian for an arbitrary electron, labeled by the two valley integer indices η and κ, which include nearest-neighbor hopping terms, takes the form

$$\hat{H} = \sum_{\eta i j} \left[-\mu_{ij}^a a_{\eta i}^\dagger a_{\eta j} - \mu_{ij}^b b_{\eta i}^\dagger b_{\eta j} \right]$$
$$+ \sum_{\langle \eta\kappa \rangle, ij} t_{\eta\kappa, ij} (a_{\eta i}^\dagger b_{\kappa j} + b_{\kappa j}^\dagger a_{\eta i}). \tag{3}$$

Here, a and b indicate the fermionic annihilation operator on the carbon atoms. The indices η and κ show the site labels in sublattices A and B, respectively, and i and j indicate the atomic orbital. The matrix elements μ^a, μ^b, and $t_{\eta\kappa, ij}$ are responsible for the on-site energies of carbon atoms and hopping between different neighboring sites, respectively. The final result for the effective tight-binding Hamiltonian governing the conduction and valence bands is given by

$$h(\mathbf{k}) = -\gamma \begin{pmatrix} 0 & f(\mathbf{k}) \\ f^*(\mathbf{k}) & 0 \end{pmatrix}. \tag{4}$$

The hopping integral $\gamma \cong 2.85$ eV is defined as the coupling between sublattices A and B, and

$$f(\mathbf{k}) = \exp(-ik_x a)\left[1 + 2\exp\left(\frac{3ik_x a}{2}\right)\cos\left(\frac{\sqrt{3}k_y a}{2}\right)\right]$$

$$\equiv |f(\mathbf{k})|e^{i\phi_{\mathbf{k}}}, \tag{5}$$

with

$$\phi_{\mathbf{k}} = \arctan\{\text{Im}[f(\mathbf{k})]/\text{Re}[f(\mathbf{k})]\},$$

which represents the structure factor of the honeycomb lattice with lattice parameter a and the wave vector of the electron $\mathbf{k}$. In the proximity-induced superconducting graphene case, the superconducting generalization of the tight-binding Hamiltonian can be written on monolayer graphene, including the pairing potential. In the relativistic case, Cooper pairing takes place between single-particle states, which are constructed by application of discrete symmetries (parity, charge conjugation, and time reversal). The possible pairing states can be characterized as singlet or triplet order parameters. The order parameter of the superconductor is defined as a function of spin (s, s') and momentum (k, k') for electrons and holes. In this paper, we consider the superconducting pair potential to be spin singlet s-wave symmetry. In the band-structure picture, the term of the interaction of the superconducting gap with the honeycomb lattice is written as follows:

$$H_S = \sum_{\langle \eta\kappa \rangle, ij} \sum_k \sum_s V_k^s a_{\eta i}^\dagger (b_{\kappa j}^\dagger + b_{\kappa j}'^\dagger) + \text{H.c.}, \tag{6}$$

where V_k^s parametrizes the pairing interaction strength of electrons, which can be determined according to the point group symmetry of graphene [52]. The related order parameter can be written as $\Delta(r) = \Delta_s e^{i\varphi}$, where Δ_s denotes the absolute value of the superconducting gap and φ is the superconducting phase. Furthermore, the s-wave superconducting gap matrix includes diagonal singlet components with respect to the index i, j.

The superconducting electron-hole quasiparticle caused by the proximity of a superconductor electrode on top of monolayer graphene can be realized by the generalization of the DBdG Hamiltonian. Finally, the resulting 4×4 DBdG Hamiltonian for the singlet components is given by

$$\mathcal{H}_0^{\text{DBdG}} = \begin{pmatrix} h(\mathbf{k}) - E_F + U(x) & \Delta_s e^{i\varphi} I_2 \\ \Delta_s^* e^{-i\varphi} I_2 & -h(\mathbf{k}) + E_F - U(x) \end{pmatrix}, \tag{7}$$

where the electrostatic potential $U(x)$ gives the relative shift of the Fermi energy E_F as $\mu_s = E_F - U(x)$, which denotes the chemical potential. The pair potential $\Delta(r) = \Delta_s e^{i\varphi}$ couples electron and hole states, and I_2 is the 2×2 unit matrix that corresponds to scalar (singlet) pairing. The globally broken $U(1)$ symmetry in the superconductor is characterized by the phase φ. Diagonalizing Eq. (7) gives the following energy quartic equation:

$$\epsilon^4 - 2\epsilon^2\left[\mu_s^2 + \gamma^2|f(\mathbf{k})|^2 + |\Delta_s|^2\right] + \left[\mu_s^2 - \gamma^2|f(\mathbf{k})|^2\right]^2$$
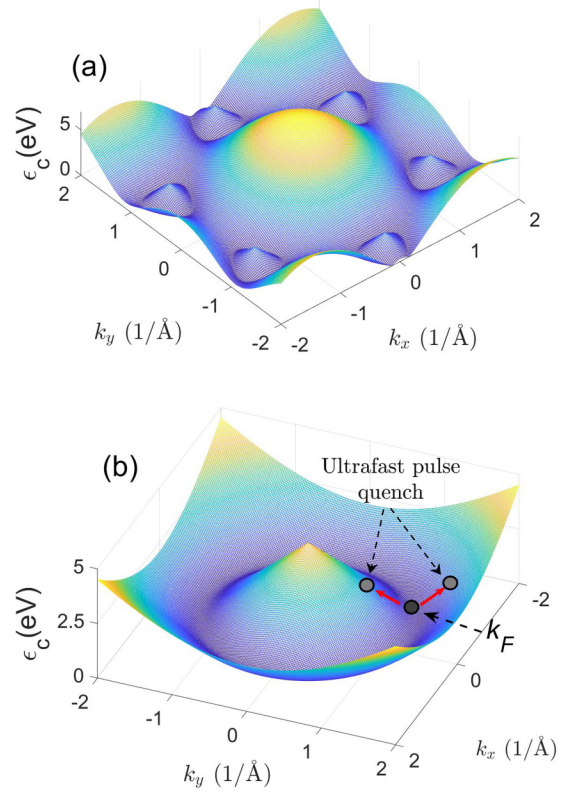$$+ |\Delta_s|^2\left[2\mu_s^2 + 2\gamma^2|f(\mathbf{k})|^2 + |\Delta_s|^2\right] = 0.$$

FIG. 4. (a) The energy spectrum is shown for a graphene superconductor as a function of k_x and k_y in the extended zone. (b) Illustration of electronlike and holelike quantum quench in the Fermi surface on the graphene superconductor. The superconducting effective gap is formed in the Fermi wave vector k_F of the Mexican hat.

The energy spectrum of DBdG for electron-hole excitations becomes

$$\epsilon_{c,v} = \pm\sqrt{[-\mu_s + \xi\gamma|f(\mathbf{k})|]^2 + |\Delta_s|^2}, \tag{8}$$

where indices c and v stand for the CB and VB, respectively. The parameter $\xi = \pm$ distinguishes between the conduction and valence bands. The energy spectrum is shown in Fig. 4(a), where the inverted band around the Dirac points denotes superconducting electron-hole excitations in honeycomb reciprocal space. The superconducting effective gap is formed in the Fermi wave vector k_F of the Mexican hat, as demonstrated in Fig. 4(b). The ultrafast optical pulse causes an impulsive excitation of Higgs oscillations via a nonlinear process by quenching the Mexican hat pair potential in superconductors [1] [see Fig. 4(b)]. In order to have Higgs oscillations in the above energy pattern, the optical pulse must fulfill the nonadiabaticity, which implies a one- to two-cycle short pulse with a frequency range in the approximately femtosecond regime.

Using the Hamiltonian (7), the four-component electronlike wave functions corresponding to the valence and conduction bands are given by

$$\psi_{\mathbf{k}}^{(c,e)} = \frac{e^{i\mathbf{k}\cdot\mathbf{r}}}{\sqrt{\alpha_1}} \begin{pmatrix} \beta_1 e^{i\phi_{\mathbf{k}}} \\ -\beta_1 \\ \lambda_1 e^{i\phi_{\mathbf{k}}} \\ \rho_1 \end{pmatrix}, \quad \psi_{\mathbf{k}}^{(v,e)} = \frac{e^{i\mathbf{k}\cdot\mathbf{r}}}{\sqrt{\alpha_1}} \begin{pmatrix} \beta_1 e^{i\phi_{\mathbf{k}}} \\ \beta_1 \\ -\rho_1 e^{i\phi_{\mathbf{k}}} \\ \lambda_1 \end{pmatrix},$$

and the holelike ones are given by

$$\psi_{\mathbf{k}}^{(c,h)} = \frac{e^{i\mathbf{k}\cdot\mathbf{r}}}{\sqrt{\alpha_2}}\begin{pmatrix} -\beta_2 e^{i\phi_{\mathbf{k}}} \\ \beta_2 \\ \lambda_2 e^{i\phi_{\mathbf{k}}} \\ \rho_2 \end{pmatrix}, \quad \psi_{\mathbf{k}}^{(v,h)} = \frac{e^{i\mathbf{k}\cdot\mathbf{r}}}{\sqrt{\alpha_2}}\begin{pmatrix} -\beta_2 e^{i\phi_{\mathbf{k}}} \\ -\beta_2 \\ -\rho_2 e^{i\phi_{\mathbf{k}}} \\ \lambda_2 \end{pmatrix},$$
$$(9)$$

where we have defined

$$\alpha_{1(2)} = 2\beta_{1(2)}^2 + \lambda_{1(2)}^2 + \rho_{1(2)}^2,$$

$$\beta_{1(2)} = \Delta_s\left(\frac{\sqrt{\epsilon_c^2 - |\Delta_s|^2} + (-)\mu_s}{\epsilon_c - (+)\sqrt{\epsilon_c^2 - |\Delta_s|^2}}\right),$$

and

$$\lambda_{1(2)} = \frac{|\Delta_s|^2}{\epsilon_c - (+)\sqrt{\epsilon_c^2 - |\Delta_s|^2}} - \epsilon_c + \mu_s,$$

$$\rho_{1(2)} = -\mu_s - (+)\sqrt{\epsilon_c^2 - |\Delta_s|^2}.$$

These single-particle wave functions will play a substantial role in conduction-valence band coupling via the electric dipole moment.

B. Transition probability

The electron dynamics in the external electric field of the pulse is coherent, and the electron collision effect is negligible since the electron scattering time in graphene is longer than 10 fs, which is longer than the duration of the pulse ($\sim$5 fs) [53–58]. Coherent electron dynamics in superconducting graphene can be described by the time-dependent Schrödinger equation:

$$i\hbar\frac{d\Psi(t)}{dt} = \mathcal{H}(t)\Psi(t). \tag{10}$$

The coherent electron dynamics in graphene has two major components: intraband and interband dynamics. In the reciprocal space, the intraband dynamics is described by the Bloch acceleration theorem [59], which has the following form:

$$\hbar\frac{d\mathbf{k}(t)}{dt} = e\mathbf{F}(t). \tag{11}$$

For an electron with initial wave vector $\mathbf{q}$, the electron dynamics is described by time-dependent wave vector $\mathbf{k}_T(\mathbf{q}, t)$, which can be found by the solution of Eq. (11),

$$\mathbf{k}_T(\mathbf{q}, t) = \mathbf{q} + \frac{e}{\hbar}\int_{-\infty}^{t} \mathbf{F}(t_1)dt_1. \tag{12}$$

After the pulse ends, the electron momentum deterministically returns to its original value, $\mathbf{k}_T(\mathbf{q}, t) \to \mathbf{q}$, and consequently, there can be no interference of an electron wave with itself. The corresponding wave functions, which are the solution of the Schrödinger equation (10) within a single band, i.e., without interband coupling, are the Houston functions [60]

$$\phi_{\sigma\mathbf{q}}^{H}(\mathbf{r}, t) = \psi_{\mathbf{k}_T(\mathbf{q},t)}^{\sigma}(\mathbf{r})\exp\left[-i\int_{-\infty}^{t}dt_1\varepsilon_{\sigma}[\mathbf{k}_T(\mathbf{q}, t_1)]\right], \tag{13}$$

where the index $\sigma \equiv (c, v)$ stands for CB and VB, respectively. We express the general solution of the Schrödinger

equation by expanding in the basis of the Houston function,

$$\psi_{\mathbf{q}}(\mathbf{r}, t) = \sum_{\sigma=c,v}\Theta_{\sigma\mathbf{q}}(t)\phi_{\sigma\mathbf{q}}^{H}(\mathbf{r}, t), \tag{14}$$

where $\Theta_{\sigma\mathbf{q}}(t)$ is the corresponding time-dependent expansion coefficient, which satisfies the following coupled differential equations:

$$\frac{d\Theta_{c\mathbf{q}}(t)}{dt} = -i\frac{\mathbf{F}(t)\mathbf{Q}_{\mathbf{q}}(t)}{\hbar}\Theta_{v\mathbf{q}}(t),$$

$$\frac{d\Theta_{v\mathbf{q}}(t)}{dt} = -i\frac{\mathbf{F}(t)\mathbf{Q}_{\mathbf{q}}^{*}(t)}{\hbar}\Theta_{c\mathbf{q}}(t), \tag{15}$$

where vector functions $\mathbf{Q}_{\mathbf{q}}(t)$ are related to the interband dipole matrix elements $D(\mathbf{k})$:

$$\mathbf{Q}_{\mathbf{q}}(t) = \mathbf{D}[\mathbf{k}_T(\mathbf{q}, t)]\exp$$
$$\times\left[-\frac{i}{\hbar}\int_{-\infty}^{t}dt_1\{\varepsilon_c[\mathbf{k}_T(\mathbf{q}, t_1)] - \varepsilon_v[\mathbf{k}_T(\mathbf{q}, t_1)]\}\right], \tag{16}$$

with the electron-electron and hole-hole dipole contributions

$$\mathbf{D}^{(v,e\to c,e)}(\mathbf{k}) = \langle\psi_{\mathbf{k}}^{(c,e)}|e\mathbf{r}|\psi_{\mathbf{k}}^{(v,e)}\rangle,$$

$$\mathbf{D}^{(v,h\to c,h)}(\mathbf{k}) = \langle\psi_{\mathbf{k}}^{(c,h)}|e\mathbf{r}|\psi_{\mathbf{k}}^{(v,h)}\rangle. \tag{17}$$

Substituting the wave functions of the conduction and valence bands [Eqs. (9)] into Eqs. (17), we obtain the following expressions for the x and y components of the electric dipole matrix elements, which couple conduction and valence bands in Dirac points:

$$D_j^{[v,e(h)\to c,e(h)]}(\mathbf{k})$$
$$= \Omega_{1(2)}\left[\mathscr{Z}_j - \frac{ie}{\alpha_{1(2)}}\left(\rho_{1(2)}\frac{\partial\lambda_{1(2)}}{\partial k_j} - \lambda_{1(2)}\frac{\partial\rho_{1(2)}}{\partial k_j}\right)\right]$$
$$(j \equiv x, y), \tag{18}$$

where we have

$$\Omega_{1(2)} = \frac{1}{2\alpha_{1(2)}}\frac{\partial\alpha_{1(2)}}{\partial k_j},$$

$$\mathscr{Z}_x = \frac{ea}{2\Gamma}\left\{1 + \cos\left(\frac{\sqrt{3}ak_y}{2}\right)\right.$$
$$\left. \times\left[\cos\left(\frac{3ak_x}{2}\right) - 2\cos\left(\frac{\sqrt{3}ak_y}{2}\right)\right]\right\},$$

$$\mathscr{Z}_y = \frac{ea\sqrt{3}}{2\Gamma}\sin\left(\frac{\sqrt{3}ak_y}{2}\right)\sin\left(\frac{3ak_x}{2}\right),$$

and

$$\Gamma = 1 + 4\cos\left(\frac{\sqrt{3}ak_y}{2}\right)\left[\cos\left(\frac{3ak_x}{2}\right) + \cos\left(\frac{\sqrt{3}ak_y}{2}\right)\right].$$

Finally, we proceed to solve numerically the set of two coupled differential equations (15) simultaneously by assuming the initial condition (for $t \to -\infty$) $(\Theta_{v\mathbf{q}}, \Theta_{c\mathbf{q}}) = (1, 0)$, which means that before applying the pulse, the VB is initially occupied and the CB is empty. We characterize the corresponding electron dynamics in terms of the CBP. For an
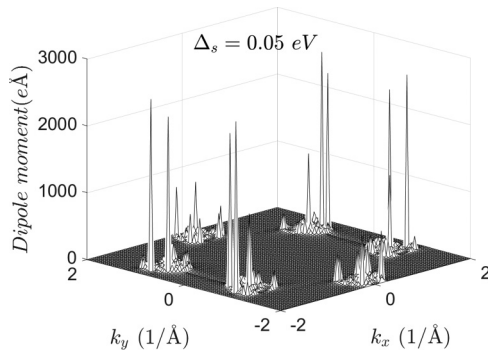
FIG. 5. Interband dipole matrix element D_x as a function of wave vectors k_x and k_y. The dipole matrix element is singular around the Dirac points (K and K' points). Also, we observe that the height and form of peaks in all Dirac points are asymmetric.

electron, which is initially in the VB, the mixing of the states of different bands is characterized by the time-dependent expansion coefficient probability $|\Theta_{c\mathbf{q}}(t)|^2$. Finally, the time-dependent CBP can be defined as

$$\mathcal{N}_{\text{CB}}(t) = \sum_{\mathbf{q}} |\Theta_{c\mathbf{q}}(t)|^2, \tag{19}$$

where the sum is over all momenta in the first Brillouin zone and the solution $\Theta_{c\mathbf{q}}(t)$ satisfies the initial condition $(\Theta_{v\mathbf{q}}, \Theta_{c\mathbf{q}}) = (1, 0)$. This distribution is nonzero during the pulse passing, and its residual value $\mathcal{N}_{\text{CB}}^{(\text{res})}(t)$ determines the irreversibility character of the electron dynamics. In addition to the irreversibility, the residual CBP distribution $\mathcal{N}_{\text{CB}}^{(\text{res})}(t)$ will determine the valley polarization after a linearly polarized pulse.

III. NUMERICAL RESULTS AND DISCUSSION

In this section, we proceed to investigate in detail Dirac-fermion dynamics in superconducting graphene interacting with a femtosecond pulse. In particular, the specific feature of our proposed system is characterized by the interplay between electron-hole excitations and the optical pulse in graphene via ultrafast electron dynamics. This is possible by numerically solving the set of coupled differential equations (15) simultaneously, with the initial condition $(\Theta_{v\mathbf{q}}, \Theta_{c\mathbf{q}}) = (1, 0)$. This may exactly determine the evolution of the electron states and, correspondingly, the charge transition rate of the system associated with the CBP. Furthermore, the interband electron dynamics is characterized by electron redistribution between the valence and conduction bands after the pulse ends. The results obtained are presented and discussed below. First, we expect that the valence and conduction bands are coupled by the electric field of the pulse via an electric dipole moment given by Eqs. (17). By analytical solution, we arrive at a complex expression for the dipole moment [Eq. (18)]. The imaginary part can originate from the presence of the superconductor gap in the system. Thus, we need to calculate the absolute value of the dipole moment. The result is demonstrated in Fig. 5, where we see sharp peaks as singularities around Dirac points in the honeycomb lattice. There is no coupling at the center of the Brillouin zone. Importantly, there

are several peaks in each Dirac point, which actually result from the exciting Higgs oscillations of the superconducting order following the pulse. The dipole moment peaks occur not exactly in Dirac points but in Fermi points, where the superconducting gap forms in graphene, as shown in Fig. 4(b). Also, we see that the height and form of peaks in all Dirac points have no symmetric pattern. In fact, this can be understood to be a result of the reduction of the point group symmetry of the honeycomb lattice, that is, C_{6v}, upon irradiation with an electric field along the x direction. As pointed out, the mirror symmetry $x \to -x$ is broken, but the mirror symmetry $y \to -y$ still survives as a residual mirror symmetry. This residual symmetry is clearly seen in the dipole excitation profile. Consequently, such a feature can lead to a significant valley polarization effect in these systems (which was also clearly reported for 2D materials without the presence of a superconducting gap [21,61]). Therefore, our understanding of valley polarization in our proposed system can arise from the breaking of the mirror symmetry $x \to -x$.

Now, our investigation is focused on exploring the effect of the superconducting gap magnitude Δ_s and optical pulse intensity F_0 on the CBP. It is important to note that in the nonadiabatic regime, the superconducting order parameter magnitude oscillates with pulse time. The amplitude of oscillations is, nevertheless, a very small fraction of the order parameter itself [47,62]. There is yet another *a posteriori* justification to ignore the oscillations of the order parameter: As will be seen shortly, the CBP is not very sensitive even for huge changes in the superconducting order parameter. So the incremental variations in the order parameter can be ignored altogether. The probability of CBP is presented as a function of time for a pulse duration with one to two cycles in Figs. 6 and 7. The effect of pulse intensity on the CBP for the two dipole moments $D^{(v,e \to c,e)}(\mathbf{k})$ and $D^{(v,h \to c,h)}(\mathbf{k})$ (which give the major contribution to the electron-electron or hole-hole transitions) is demonstrated in Figs. 6(a) and 7(a), respectively. In the following, Figs. 6(b) and 7(b) show the CBP as a function of time for various magnitudes of pair potentials for two types transitions. First, as a key feature of coherent electron dynamics in 2D materials, the irreversible electron dynamics is achieved for the CBP. The irreversibility of the electron dynamics in superconducting graphene is due to strong interband nonlinear coupling in Dirac points. We can see that the residual CB transition has a finite value after the pulse ends. Second, we observe almost a balance in electron-electron and hole-hole transitions. Here, we deduce from Figs. 6(a) and 7(a) that the maximum and minimum residual CBPs for $F_0 = 1.5$ V/Å and $F_0 = 0.5$ V/Å are obtained, respectively. The residual CBP is very sensitive to the strength of the pulse. Moreover, as the pair potential can oscillate with THz pulse irradiation (due to the Higgs mode), we proceed to investigate its effect on the CBP. To clarify, we theoretically vary the pair potential magnitude in electronlike or holelike CB transitions, as shown in Figs. 6(b) and 7(b). We see that the residual CBP is weakly sensitive to the magnitude of Δ_s. This result seems to be obvious as the varying pair potential actually adjusts the amount of the effective superconducting gap at the Fermi surface of the Mexican hat. To see the role of the superconducting gap more clearly, we plot in Fig. 8 the ratio of the dipole moment excitations resulting from the
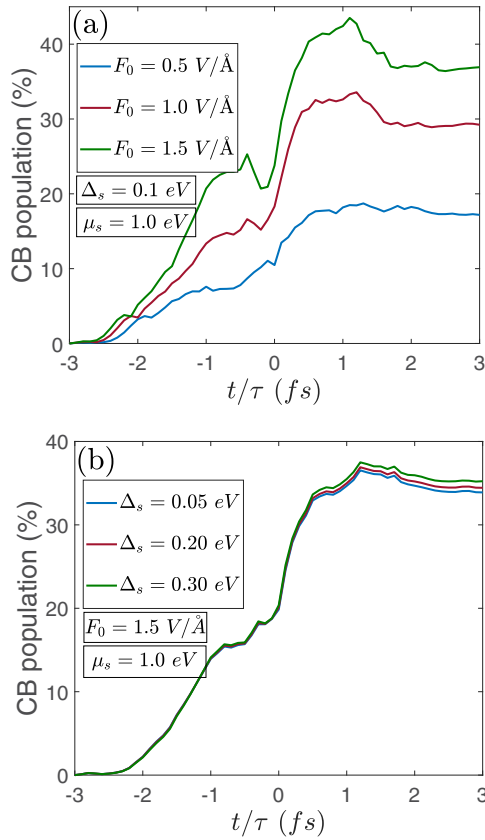
FIG. 6. Plot of CBP probability as a function of time for (a) different amplitudes of F_0 and (b) different amounts of Δ_s for $D^{(v,e \to c,e)}(\mathbf{k})$. For all states we take pulse incident angle $\theta = 0$.

FIG. 7. The same as in Fig. 6, but for $D^{(v,h \to c,h)}(\mathbf{k})$.

nonlinear conduction-valence band coupling. One can see that upon changing Δ_s from 0.01 to 0.05 eV, the ratio of the dipole moment is strongly enhanced for some peaks around Dirac points. This can be viewed as an indirect fingerprint of the highly nonlinearly excited Higgs mode in the dipole pattern near the Dirac hot spots (see Fig. 9). Furthermore, the formation of such hot spots around the Dirac nodes signifies the importance of Dirac-type band touching in enhancing the highly nonlinear Higgs excitations by ultrashort pulses. In other words, the band touching at the Dirac node facilitates the excitations of Higgs modes of a few meV by eV pulses and leaves a clear signature in the interband dipole pattern.

Accordingly, the redistribution of electrons around two types of Dirac valleys (K and K') when the pulse ends can more clearly unveil the effective coherent electron dynamics in the presence of a superconductor, giving rise to the practically important total charge transfer rate. To this end, we proceed to evaluate the residual CBP distribution, for which we take the summation of the CBP probability over all time-dependent electron momenta in the first Brillouin zone. The signature of the superconducting gap magnitude and pulse intensity in the CB redistribution of electrons around the Dirac points are shown. The residual CB distribution $\mathcal{N}_{\mathrm{CB}}^{(\mathrm{res})}(t)$ of electrons in the reciprocal space is represented in Figs. 9(a)– 9(c) for dipole moment $D^{(v,e \to c,e)}(\mathbf{k})$. In Figs. 9(a) and 9(b), the distribution of the residual CBP is given for two different pulse amplitudes, $F_0 = 0.5$ and 1 V/Å, respectively. We
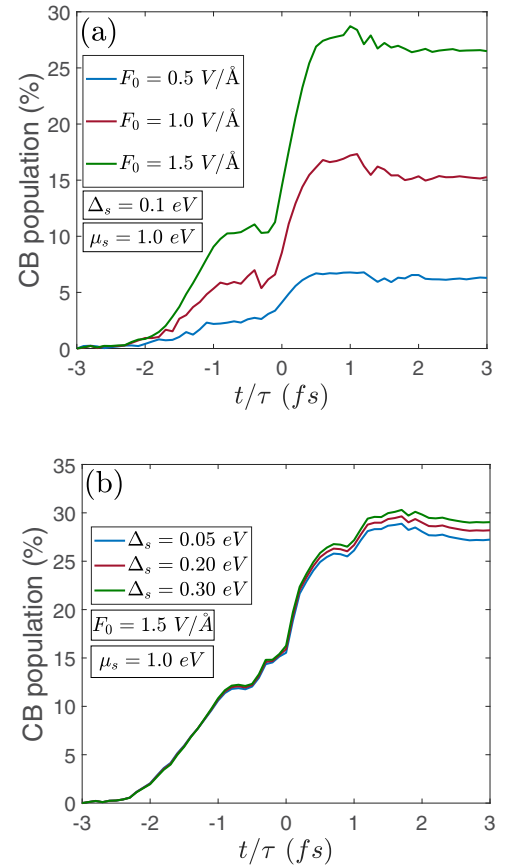
deduce that the hot spots related to the electron distribution in the corners of the first Brillouin zone are enhanced by the increase in the pulse intensity. An asymmetric electron distribution with respect to the K and K' valleys is more or less observed with a mirror symmetry pattern. This result can be compared with the same system without a superconductor (see Ref. [18]). Importantly, this can lead to the valley polarization effect, which may originate from the effect of the
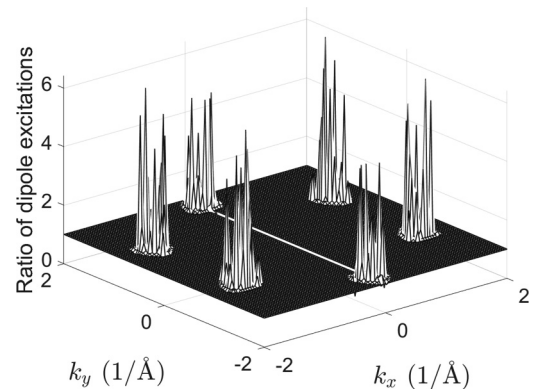

FIG. 8. Plot of the ratio of dipole moment excitations resulting from the nonlinear coupling of radiation with superconducting graphene upon changing Δ_s from 0.01 to 0.05 eV. Some peaks associated with the Higgs oscillations around Dirac points are enhanced.
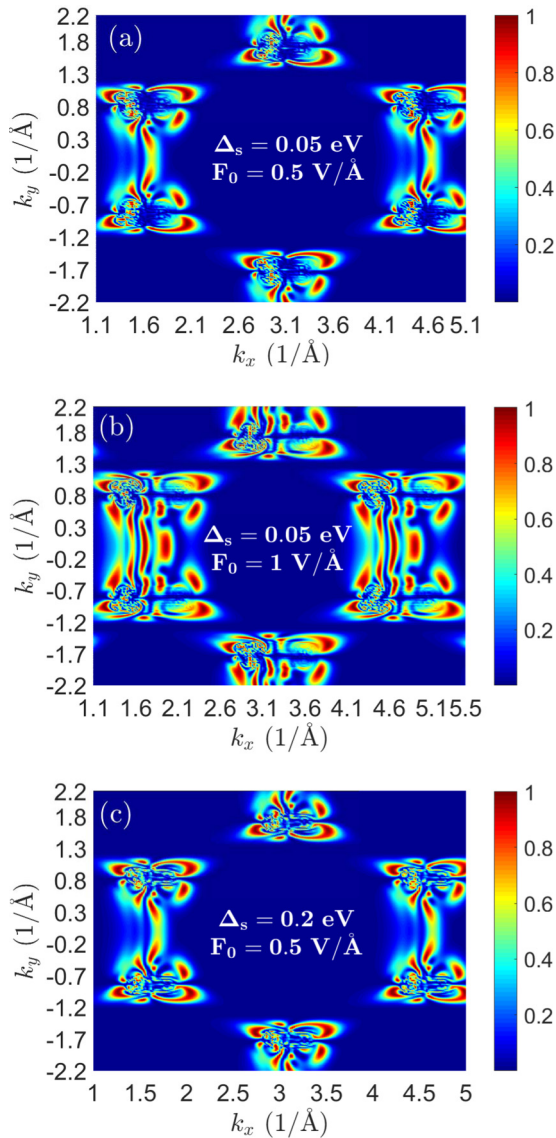
FIG. 9. CB electron distribution in the proximity of Dirac points after the pulse ends as a function of wave vectors k_x and k_y for different values of F_0 and Δ_s for (a) $F_0 = 0.5$ V/Å, $\Delta_s = 0.05$ eV, (b) $F_0 = 1$ V/Å, $\Delta_s = 0.05$ eV, and (c) $F_0 = 0.5$ V/Å, $\Delta_s = 0.2$ eV for $D^{(v,e \to c,e)}(\mathbf{k})$. Only the first Brillouin zone is shown.

superconducting order in the inequivalent valleys in graphene. The effect of varying the pair potential on the CB electron redistribution at the Dirac points is presented in Fig. 9(c). Here, we see that the hot spots are slightly enhanced near the Dirac points by the increase in Δ_s in a high range up to 0.2 eV. Very recently, experimental and numerical demonstrations of the interband electron transition and also the effect of superconductivity on coherent electron dynamics in a strong field (≈ 1 V/Å) were realized (see Refs. [4,6,31,32,47]). Our exact numerical results can be compared with the experimental reports and can open up ways to extend the optoelectronic applications and ultrafast information processing in the THz domain.

These hot spots can be directly observed by time-resolved angle-resolved photoemission spectroscopy (tr-ARPES)

experiments. The observed patterns of tr-ARPES are in good agreement with calculations [63].

IV. CONCLUSION AND OUTLOOK

In summary, we have analytically investigated electron dynamics in proximity to superconducting graphene under ultrashort pulse irradiation by taking the s-wave pairing symmetry into account. The electron-hole dynamics of the system was considered to be coherent and nonadiabatic because the duration of a few femtosecond pulse with an amplitude of the order of 0.1–1 V/Å is less than the electron scattering time in graphene. The electric dipole matrix moment of the system, which couples electron-electron or hole-hole from the VB to the CB, was found to be a complex function owing to the existence of superconductivity. An impulsive excitation of Higgs oscillations via a nonlinear process by quenching the Mexican hat of superconducting excitations was found to affect valence-conduction band coupling by the pulse. The singularity arising from the band touching at the Dirac point gives a dominant role to the interband dipole excitations around the Dirac nodes. Due to the scale invariance of the Dirac theory, this feature will persist even with THz pulses. However, in that regime the dynamics of electrons and holes cannot be assumed to be coherent, as they experience many collisions during a pulse period. By varying the size of the superconducting gap, we find that the ratio of interband dipoles is enhanced by a factor of 2–6. This signifies the indirect role of Higgs excitations in the resulting dipole moments. We have demonstrated in detail the effect of the superconducting gap and pulse intensity on the CBP during the time the pulse is applied and also after it ends. Particularly, the irreversible electron and hole dynamics was achieved as a noticeable phenomenon in 2D Dirac materials, and the maximum CBP almost occurs in its residue. Remarkably, we have found an asymmetric electron redistribution for two different Dirac points as degenerate K and K' valleys, controlled by the superconducting gap and pulse intensity. We ascribe the resulting valley asymmetry to the breaking of the $x \to -x$ mirror symmetry of the parent graphene material that results from the strong coupling of the radiation and graphene electrons. Therefore, our findings clearly reveal the valley polarization effect associated with the nonlinear excitations of the Higgs mode in graphene. Finally, our results have shown that the interaction of graphene subjected to a superconductivity order with ultrashort optical pulse can exhibit behaviors distinct from the other solids, which can be attributed to the band touching at the Dirac nodes.

Since the duration of the pulses is assumed to be less than the electron scattering time, the electron dynamics on this timescale remains coherent, and photoexcited electrons do not have time to get scattered off each other and impurities, and therefore, the heating and dissipation in this regime can be ignored. One must also note that since the ultrashort pulses are tantamount to a broad frequency spectrum, the whole electronic band structure is engaged in the nonlinear excitation process. Among so many degrees of freedom, those lying close to Fermi level are described in the superconducting state by the Bogoliubov–de Gennes theory. As such, the present study serves to illustrate how the pairing at low energy around the Fermi level affects the ultrafast electron dynamics in graphene.

[1] R. Shimano and N. Tsuji, Annu. Rev. Condens. Matter Phys. **11**, 103 (2020)

[2] A. Schiffrin, T. Paasch-Colberg, N. Karpowicz, V. Apalkov, D. Gerster, S. Muhlbrandt, M. Korbman, J. Reichert, M. Schultze, S. Holzner, J. V. Barth, R. Kienberger, R. Ernstorfer, V. S. Yakovlev, M. I. Stockman, and F. Krausz, Nature (London) **493**, 70 (2012).

[3] V. Apalkov and M. I. Stockman, Phys. Rev. B **86**, 165118 (2012).

[4] T. Higuchi, C. Heide, K. Ullmann, H. B. Weber, and P. Hommelho, Nature (London) **550**, 224 (2017).

[5] S. A. O. Motlagh, V. Apalkov, and M. I. Stockman, Phys. Rev. B **95**, 085438 (2017).

[6] C. Heide, T. Higuchi, H. B. Weber, and P. Hommelhoff, Phys. Rev. Lett. **121**, 207401 (2018).

[7] H. Z. Liu, Y. L. Li, Y. S. You, S. Ghimire, T. F. Heinz, and D. A. Reis, Nat. Phys. **13**, 262 (2017).

[8] J. Zhang, H. Ouyang, X. Zheng, J. You, R. Chen, T. Zhou, Y. Sui, Y. Liu, X. Cheng, and T. Jiang, Opt. Lett. **43**, 243 (2018).

[9] A. Kaiser, B. Rethfeld, M. Vicanek, and G. Simon, Phys. Rev. B **61**, 11437 (2000).

[10] F. Nematollahi, S. A. Oliaei Motlagh, V. Apalkov, and M. I. Stockman, Phys. Rev. B **99**, 245409 (2019).

[11] M. Lenzner, J. Kruger, S. Sartania, Z. Cheng, C. Spielmann, G. Mourou, W. Kautek, and F. Krausz, Phys. Rev. Lett. **80**, 4076 (1998).

[12] M. Gertsvolf, M. Spanner, D. M. Rayner, and P. B. Corkum, J. Phys. B **43**, 131002 (2010).

[13] M. Schultze, E. M. Bothschafter, A. Sommer, S. Holzner, W. Schweinberger, M. Fiess, M. Hofstetter, R. Kienberger, V. Apalkov, V. S. Yakovlev, M. I. Stockman, and F. Krausz, Nature (London) **493**, 75 (2013).

[14] O. Kwon, T. Paasch-Colberg, V. Apalkov, B.-K. Kim, J.-J. Kim, M. I. Stockman, and D. E. Kim, Sci. Rep. **6**, 21272 (2016).

[15] A. K. Geim and K. S. Novoselov, Nat. Mater. **6**, 183 (2007).

[16] A. H. Castro Neto, F. Guinea, N. M. R. Peres, K. S. Novoselov, and A. K. Geim, Rev. Mod. Phys. **81**, 109 (2009).

[17] S. Z. Butler *et al.*, ACS Nano **7**, 2898 (2013).

[18] H. Koochaki Kelardeh, V. Apalkov, and M. I. Stockman, Phys. Rev. B **91**, 045439 (2015).

[19] H. K. Kelardeh, V. Apalkov, and M. I. Stockman, Phys. Rev. B **96**, 075409 (2017).

[20] F. Nematollahi, V. Apalkov, and M. I. Stockman, Phys. Rev. B **97**, 035407 (2018).

[21] S. A. O. Motlagh, J. S. Wu, V. Apalkov, and M. I. Stockman, Phys. Rev. B **98**, 081406(R) (2018).

[22] S. Pashalou, H. Goudarzi, and M. Khezerlou, J. Phys.: Condens. Matter **32**, 355403 (2020).

[23] J. Reimann, S. Schlauderer, C. P. Schmid, F. Langer, S. Baierl, K. A. Kokh, O. E. Tereshchenko, A. Kimura, C. Lange, J. Gudde, U. Hofer, and R. Huber, Nature (London) **562**, 396 (2018).

[24] H. K. Kelardeh, V. Apalkov, and M. I. Stockman, Phys. Rev. B **92**, 045413 (2015).

[25] M. Trushin, A. Grupp, G. Soavi, A. Budweg, D. De Fazio, U. Sassi, A. Lombardo, A. C. Ferrari, W. Belzig, A. Leitenstorfer, and D. Brida, Phys. Rev. B **92**, 165429 (2015).

[26] E. Gruber *et al.*, Nat. Commun. **7**, 13948 (2016).

[27] D. Sun, G. Aivazian, A. M. Jones, J. S. Ross, W. Yao, D. Cobden, and X. Xu, Nat. Nanotechnol. **7**, 114 (2012).

[28] S. A. O. Motlagh, A. J. Zafar, A. Mitra, V. Apalkov, and M. I. Stockman, Phys. Rev. B **101**, 165433 (2020).

[29] H. K. Kelardeh, V. Apalkov, and M. I. Stockman, Phys. Rev. B **93**, 155434 (2016).

[30] S. Pashalou and H. Goudarzi, Superlattices Microstruct. **144**, 106566 (2020).

[31] C. Heide, T. Boolakee, T. Higuchi, H. B. Weber, and P. Hommelhoff, New J. Phys. **21**, 045003 (2019).

[32] C. Heide, T. Boolakee, T. Higuchi, and P. Hommelhoff, J. Phys. Photonics **2**, 024004 (2020).

[33] K. S. Novoselov, A. K. Geim, S. V. Morozov, D. Jiang, M. I. Katsnelson, I. V. Grigorieva, S. V. Dubonos, and A. A. Firsov, Nature (London) **438**, 197 (2005).

[34] J. Linder and A. Sudbo, Phys. Rev. B **77**, 064507 (2008).

[35] J. Linder, A. M. Black-Schaffer, T. Yokoyama, S. Doniach, and A. Sudbo, Phys. Rev. B **80**, 094522 (2009).

[36] C. W. J. Beenakker, Phys. Rev. Lett. **97**, 067007 (2006).

[37] C. W. J. Beenakker, Rev. Mod. Phys. **80**, 1337 (2008).

[38] H. B. Heersche, P. Jarillo-Herrero, J. B. Oostinga, L. M. K. Vandersypen, and A. F. Morpurgo, Nature (London) **446**, 56 (2007).

[39] X. Du, I. Skachko, and E. Y. Andrei, Phys. Rev. B **77**, 184507 (2008).

[40] A. Yu. Kasumov, R. Deblock, M. Kociak, B. Reulet, H. Bouchiat, I. I. Khodos, Yu. B. Gorbatov, V. T. Volkov, C. Journet, and M. Burghard, Science **284**, 1508 (1999).

[41] A. F. Morpurgo, J. Kong, C. M. Marcus, and H. Dai, Science **286**, 263 (1999).

[42] M. R. Buitelaar, W. Belzig, T. Nussbaumer, B. Babic, C. Bruder, and C. Schonenberger, Phys. Rev. Lett. **91**, 057005 (2003).

[43] R. Matsunaga and R. Shimano, Phys. Rev. Lett. **109**, 187002 (2012).

[44] R. Matsunaga, Y. I. Hamada, K. Makise, Y. Uzawa, H. Terai, Z. Wang, and R. Shimano, Phys. Rev. Lett. **111**, 057002 (2013).

[45] R. Matsunaga *et al.*, Science **345**, 1145 (2014).

[46] R. Matsunaga, N. Tsuji, K. Makise, H. Terai, H. Aoki, and R. Shimano, Phys. Rev. B **96**, 020505(R) (2017).

[47] L. Schwarz, B. Fauseweh, N. Tsuji, N. Cheng, N. Bittner, H. Krull, M. Berciu, G. S. Uhrig, A. P. Schnyder, S. Kaiser, and D. Manske, Nat. Commun. **11**, 287 (2020).

[48] M. Claassen, D. M. Kennes, M. Zingl, M. A. Sentef, and A. Rubio, Nat. Phys. **15**, 766 (2019).

[49] A. M. Black-Schaffer and S. Doniach, Phys. Rev. B **75**, 134512 (2007).

[50] R. Nandkishore, L. Levitov, and A. Chubukov, Nat. Phys. **8**, 158 (2011).

[51] M. L. Kiesel, C. Platt, W. Hanke, D. A. Abanin, and R. Thomale, Phys. Rev. B **86**, 020507(R) (2012).

[52] E. Kogan and V. U. Nazarov, Phys. Rev. B **85**, 115418 (2012).

[53] E. H. Hwang and S. Das Sarma, Phys. Rev. B **77**, 195412 (2008).

[54] M. Breusing, S. Kuehn, T. Winzer, E. Malic, F. Milde, N. Severin, J. P. Rabe, C. Ropers, A. Knorr, and T. Elsaesser, Phys. Rev. B **83**, 153410 (2011).

[55] E. Malic, T. Winzer, E. Bobkin, and A. Knorr, Phys. Rev. B **84**, 205406 (2011).

[56] D. Brida, A. Tomadin, C. Manzoni, Y. J. Kim, A. Lombardo, S. Milana, R. R. Nair, K. S. Novoselov, A. C. Ferrari, G. Cerullo, and M. Polini, Nat. Commun. **4**, 1987 (2013).

[57] I. Gierz, J. C. Petersen, M. Mitrano, C. Cacho, I. C. Turcu, E. Springate, A. Stohr, A. Kohler, U. Starke, and A. Cavalleri, Nat. Mater. **12**, 1119 (2013).

[58] A. Tomadin, D. Brida, G. Cerullo, A. C. Ferrari, and M. Polini, Phys. Rev. B **88**, 035430 (2013).

[59] F. Bloch, Z. Phys. A **52**, 555 (1929).

[60] W. V. Houston, Phys. Rev. **57**, 184 (1940).

[61] S. Pashalou and H. Goudarzi, J. Phys. D **53**, 465110 (2020).

[62] T. Papenkort, V. M. Axt, and T. Kuhn, Phys. Rev. B **76**, 224522 (2007).

[63] Y. Liu, G. Bian, T. Miller, and T.-C. Chiang, Phys. Rev. Lett. **107**, 166803 (2011).